1-1-2016

Size optimization of a magnetic system for drug delivery with capsule robots

Fredy Munoz
University of Wollongong, ffm517@uowmail.edu.au

Gursel Alici
University of Wollongong, gursel@uow.edu.au

Weihua Li
University of Wollongong, weihuali@uow.edu.au

Metin Sitti
Max Planck Institute for Intelligent Systems, Stuttgart, sitti@is.mpg.de

Size optimization of a magnetic system for drug delivery with capsule robots

Abstract

In this paper, we present a methodology for the size optimization of an external magnetic system made of arc-shaped permanent magnets (ASMs). This magnetic system is able to remotely actuate a drug-release module embedded in a prototype of a capsule robot. The optimization of the magnetic system is carried out by using an accurate analytical model that is valid for any arbitrary dimensions of the ASMs. By using this analytical model, we perform parametric studies and conduct a statistical analysis [analysis of variance (ANOVA)] to investigate efficient ways to distribute the volume of the ASMs so that the dimensions and volume of the magnetic system are minimized while optimal flux densities and magnetic torques are obtained to actuate the drug delivery system (DDS). The ANOVA results, at 5% significance level, indicate that changes in the angular width followed by changes in the length of the ASMs have the highest impact on the magnetic linkage. Furthermore, our experimental results, which are in agreement with the analytical results, show that the size optimization of the magnetic system is effective for the actuation of the DDS in capsule robots.

Keywords

capsule, delivery, robots, drug, size, system, magnetic, optimization

Disciplines

Engineering | Science and Technology Studies

Publication Details

Munoz, F., Alici, G., Li, W. & Sitti, M. (2016). Size optimization of a magnetic system for drug delivery with capsule robots. IEEE Transactions on Magnetics, 52 (5), 5100411-1-5100411-11.

Size Optimization of a Magnetic System for Drug Delivery with Capsule Robots

Fredy Munoz[1,2], Gursel Alici[1,2,3], Weihua Li[1,2], and Metin Sitti[4]

[1]Intelligent Nano-Tera Systems Research Laboratory, University of Wollongong, Wollongong, NSW 2522, Australia
[2]School of Mechanical, Material and Mechatronic Engineering, University of Wollongong, Wollongong, NSW 2522, Australia
[3]ARC Centre of Excellence for Electromaterials Science, University of Wollongong, Wollongong, NSW 2522, Australia
[4]Max Planck Institute for Intelligent Systems, Stuttgart, Germany

In this paper, we present a methodology for the size optimization of an external magnetic system made of arc-shaped permanent magnets (ASMs). This magnetic system is able to remotely actuate a drug release module embedded in a prototype of capsule robot. The optimization of the magnetic system is carried out by using an accurate analytical model that is valid for any arbitrary dimensions of the ASMs. By using this analytical model, we perform parametric studies and conduct a statistical analysis (ANOVA) to investigate efficient ways to distribute the volume of the ASMs so that the dimensions and volume of the magnetic system are minimized while optimal flux densities and magnetic torques are obtained to actuate the drug delivery system (DDS). The ANOVA results, at 5% significance level, indicate that changes in the angular width followed by changes in the length of the ASMs have the highest impact on the magnetic linkage. Furthermore, our experimental results, which are in agreement with the analytical results, show that the size optimization of the magnetic system is effective for the actuation of the DDS in capsule robots.

***Index Terms*—Capsule robot, drug delivery, magnetic actuation, permanent magnets.**

I. Introduction

MAGNETIC coupling systems are used in many applications due to providing i) physical isolation between the driver magnetic source and the driven load, ii) no requirements for lubrication, and (iii) non-destructive torque overload [1]. The use of different magnetic coupling forms for actuation systems in biomedical applications have become an important area of research because such magnetic systems present no harm to living tissues [2, 3].

Magnetic forces and torques are commonly used in the actuation of a variety of mechanisms. For instance, in a tetherless robotic intervention presented in [4], an electromagnet (i.e., an MRI machine) is used as the driving magnetic system that exerts a magnetic force on a driven load that is connected to a needle. In another medical application, Wireless Capsule Endoscopy (WCE), magnetic coupling has been used to remotely actuate different mechanisms embedded in prototypes of robotic capsules. It is envisaged that such mechanisms can enhance the existing WCE's capability as a complementary diagnostic medical tool [5] and may allow medical practitioners to perform more complex procedures such as biopsy [2, 6] and wireless insufflation [7].

Corresponding author: G. Alici (e-mail: gursel@uow.edu.au). Tel.: +61 2-4221-4145; fax: +61 2-4221-5474.

Color versions of one or more of the figures in this paper are available online at http://ieeexplore.ieee.org.

Digital Object Identifier (inserted by IEEE).

The magnetic actuation in WCE has been achieved by housing driven permanent magnets in the capsule endoscope (CE), called internal permanent magnets (IPMs), which interact with an external magnetic system (i.e., the driving magnetic system) that is placed outside the patient's body. For example, a ring-shaped IPM to control the trajectory of a CE was used in [8, 9], ring-shaped IPMs to deploy legs as a locomotion system for a CE were used in [10, 11], cylindrical IPMs for biopsy purposes were used in [2, 6] and two spherical IPMs to achieve wireless insufflation were employed in [7]. Furthermore, two cylindrical IPMs to release drug from a chamber in a prototype of CE were reported in [12, 13].

These proof-of-concept magnetic systems in WCE have shown that it is possible to remotely control different mechanisms embedded in a CE, thus eliminating the need of housing batteries and micromotors that occupy an important volume of the limited space of 3.0 cm^3 in the existing CE [14]. However, if these prototypes are to be implemented in a more realistic environment, larger operating distances between the driver and the driven magnets and further miniaturization of the driven magnets are required [15]. Therefore, the optimization of both the driver and driven magnets are important to overcome these two limitations. However, the optimization of the driving magnetic system to create optimal magnetic linkages has been neglected in the research on capsule robots. Thus, we present in this paper the optimization of a driving magnetic system to obtain an efficient magnetic

linkage (i.e., an optimized magnetic torque imparted to the IPM) while overcoming the aforementioned limitations.

Specifically, we focus on the size optimization of a driving magnetic system which consists of an array of arc-shaped permanent magnets (ASMs) that we have proposed to release drug in WCE [16]. This driving magnetic system generates a rotating magnetic field that imparts a magnetic torque to a small IPM that is placed in a prototype of CE and actuates a slider-crank mechanism to release drug. In our previous work, we have only optimized the angular positions of ASMs [17] to improve the magnetic linkage. However, the primary contributions in this work are: the size optimization of ASMs (i.e., thickness, angular width and length) and determining the impact on the magnetic linkage due to changes in the dimensions of ASMs. These are carried out by using analytical solutions which allow fast global optimization and are more efficient and capable of facilitating physical understanding, than the time consuming finite-element methods [18, 19]. Additionally, we use a statistical analysis (i.e., ANOVA) to determine the order of priority in which the dimensions of the ASMs should be changed to obtain efficient magnetic linkages. Although we present in this work for the first time the size optimization of a driving magnetic system to specifically actuate a drug delivery system (DDS) for WCE, the results and conclusions can be also applied to actuate different on-board mechanisms in magnetic capsule robots.

The remainder of this paper is organized as follows. Section II provides the details of the magnetomechanical system under study to achieve drug release. Section III presents the analytical models used for the optimization of the driving magnetic system to improve the magnetic field and torque. Section IV provides the verification of the analytical models with experimental results for magnetic field and also presents the optimization of the magnetic system (theoretical and experimental results). Section V presents the magnetic flux density generated by practical magnetic structures and the torque imparted to the IPM (theory and experiments). Finally, discussions of the results and future work are presented in Section VI.

II. MAGNETOMECHANICAL SYSTEM

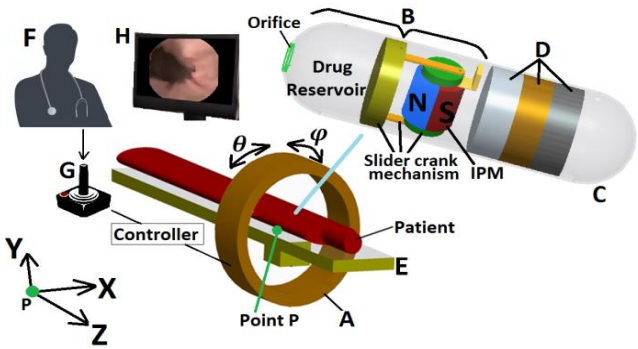

Fig. 1. The main components of the proposed drug delivery system for WCE. A: ring-shaped external magnetic system, B: drug release module, C: the robotic capsule, D: complementary modules within the capsule (anchoring mechanism, active locomotion system and localization and orientation detection module), E: patient bed, F: clinician, G: joystick, H: Human Capsule Interface. Point P represents the origin of the general coordinate system XYZ, θ is taken with respect to the x axis, and φ is taken with respect to the z axis.

Figure 1 shows a ring-shaped external magnetic system (i.e., the driving magnetic system) that produces a rotating magnetic field around the patient bed when it is physically rotated about the z axis. Although different shapes can be chosen for the IPM, cubic and cylindrical IPMs are the most commonly used for magnetic actuation in medical applications [2, 6-8, 10-12, 20]. In this work, a small cubic IPM is placed in the prototype of a capsule. This IPM is rotated by the external rotational magnetic field which is created by an array of arc-shaped permanent magnets (A_i, i=1,2,3,4) as shown in Fig. 2. The rotational movement of the IPM is then converted into a translational movement by a slider-crank mechanism that is physically connected to the IPM. In this way, a piston will push drug out of a reservoir when the external magnet is rotated around the patient's body as shown in Fig. 1.

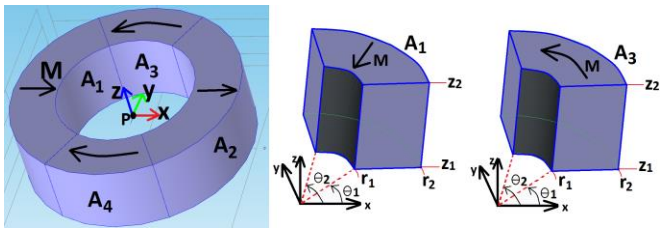

(a) (b) (c)

Fig. 2. (a) The external magnetic system implemented in this study made of arc-shaped magnets A_i, i=1,2,3,4. Parameters of an arc-shaped permanent magnet: (b) a radially magnetized segment and (c) a tangentially magnetized segment.

The driving magnetic system, the IPM and the slider-crank mechanism are the main components of this drug release mechanism. However, other modules such as active locomotion [21, 22], localization [23-25] and an anchoring mechanism are necessary in WCE to work together with the drug release module to achieve on-demand targeted drug delivery. For instance, once the CE has been taken to the region of interest in the digestive system by means of the active locomotion system, the anchoring mechanism must be activated to secure the CE in the specific position and resist the peristaltic force. The localization system could be used to determine the position and orientation of the CE and would help to make any adjustment that may be needed for the driving magnetic system to actuate the drug release mechanism. Although these additional modules should be compatible with the magnetic system that we use to accomplish drug release in WCE, they are not our focus of interest in this work. Therefore, we aim to optimize the dimensions of the arc-shaped permanent magnets (i.e., thickness: $\Delta\mathbf{r}$, angular width: $\Delta\boldsymbol{\theta}$, and length: $\Delta\mathbf{z}$) to obtain an optimized magnetic field at the centre of the system where the IPM is located and subsequently obtain an optimized magnetic torque driving the drug delivery mechanism.

The centre of the system, called point P in Fig. 2 (a), is located at the centre of a circle with a radius of r_1. The thickness of each arc-shaped magnet $\Delta\mathbf{r}$ is given by the difference between their external and internal radii, r_2 and r_1, respectively as shown in Fig. 2 (b) and (c). The length of each segment is $\Delta\mathbf{z}$=z_2-z_1, and its angular width is given by $\Delta\boldsymbol{\theta} = \boldsymbol{\theta_2} - \boldsymbol{\theta_1}$. We also use $\boldsymbol{\theta_p} = (\boldsymbol{\theta_1}+\boldsymbol{\theta_2})/\mathbf{2}$ to indicate the angular position of the centre of the ASM in the circle of radius (r_1+r_2)/2. The magnetization vector $\mathbf{M}$ could be pointing in either the radial or tangential direction as shown in Fig. 2. Furthermore, the radial direction could point toward the centre of the system (i.e., $\mathbf{M} = -|\mathbf{M}|\boldsymbol{\mu_r}$ for A_1) or outward the centre of it (i.e., $\mathbf{M} = +|\mathbf{M}|\boldsymbol{\mu_r}$ for A_2). Similarly, the tangential magnetization could be in the clockwise direction (i.e., $\mathbf{M} = -|\mathbf{M}|\boldsymbol{\mu_\theta}$ for A_4) or in the counterclockwise direction (i.e., $\mathbf{M} = +|\mathbf{M}|\boldsymbol{\mu_\theta}$ for A_3). $\boldsymbol{\mu_r}$ and $\boldsymbol{\mu_\theta}$ represent the unit vectors in a cylindrical coordinate system and $|\mathbf{M}|$ represents the magnetization grade of the permanent magnet. Finally, the notation $\mathbf{A_i^{\theta_p}}$ is used to indicate that the centre of A_i is located at the angular position given by $\boldsymbol{\theta_p}$. For instance, $\mathbf{A_1^{180^0}}$ indicates that the ASM A_1 is centred at the angular position of 180^0.

In a real application, the IPM can be off the centre and tilted as it will move along with the CE. However, for the sake of simplicity, the optimization of the driving magnetic system is carried out by assuming that it can only rotate about the z axis and that the IPM is concentric with the driving magnetic system [16]. The IPM's centre is also located at point P and can freely rotate about the z axis. The assessment of the magnetic torque imparted to the IPM and how it is affected by changes in the IPM's location and orientation are out of the scope of this paper. Nevertheless, such assessment can be conducted by using finite-element methods or analytical solutions. In Section V, we briefly analyzed the effects on the transmitted torque due to changes in the IPM's location along the x axis, however a thoroughly analysis along the 3 axis (X,Y,Z) is left for future work. In the following section, we use analytical solutions to optimize the magnetic field at the centre of the system.

III. ANALYTICAL MODELS

The magnetic torque, $\boldsymbol{\tau}$, imparted on the IPM with a volume V and a magnetization vector $\mathbf{m}$ that is exposed to an adjustable external magnetic flux density $\mathbf{B}$ is given by [26]

$$\boldsymbol{\tau} = V(\mathbf{m} \times \mathbf{B})/\mu_0 \qquad [\text{Nm}] \qquad (1)$$

μ_0 is the permeability of free space (i.e., $4\boldsymbol{\pi}\mathbf{10^{-7}}\,\frac{\mathbf{H}}{\mathbf{m}}$), and the units for both magnetization and magnetic flux density are Tesla. $\mathbf{B}$ is the magnetic flux density generated by the driving magnetic system and computed at the centre of the IPM (i.e., at point P in Fig. 2). The torque $\boldsymbol{\tau}$ will tend to orient the vector $\mathbf{m}$ along $\mathbf{B}$ and may generate a rotational movement on the IPM. Eq. (1) is commonly used as an analytical model to estimate the magnetic torque imparted to IPMs in prototypes of WCE to actuate a variety of mechanisms [8, 11, 12, 27]. Since $\boldsymbol{\tau}$ is proportional to the magnitude of $\mathbf{B}$ (i.e., $|\mathbf{B}|$), an improvement in $|\mathbf{B}|$ will increase the magnitude of the transmitted torque. Therefore, we aim to maximize $|\mathbf{B}|$ at the centre of the system that also coincides with the centre of the IPM. To this end, we use analytical models to compute $|\mathbf{B}|$ and to optimize the dimensions of the ASMs (i.e., $\Delta\mathbf{r}$, $\Delta\boldsymbol{\theta}$, $\Delta\mathbf{z}$), since these three variables affect $\mathbf{B}$. Specifically, we use two analytical models and compare them with experimental results to determine the most accurate three-dimensional model to calculate $|\mathbf{B}|$ at the centre of the system. Once we select the appropriate analytical model, based on its accuracy, we use it to optimize the dimensions of the driving magnetic system.

The first analytical model, called Model1, is based on the Coulombian model for uniformly magnetized tile permanent magnets [28] and the second analytical model, called Model2, is based on the Amperian current model for radially magnetized tile permanent magnets [29, 30] and for tangentially magnetized tile permanent magnets [31]. For the sake of brevity, these analytical models are not presented in this paper but are available in [28-31]. These 3D analytical models are expressed in cylindrical coordinates as

$$\mathbf{B} = B_r\boldsymbol{\mu_r} + B_\theta\boldsymbol{\mu_\theta} + B_z\boldsymbol{\mu_z} \qquad (2)$$

Each component is a scalar function of the dimensions of the ASMs. However, we are only interested in the radial component B_r and in the tangential component B_θ, since only these two components will tend to rotate the IPM about the z axis. In the next two subsections, we compare these two models in estimating the magnetic flux density at the centre of the system (x=y=z=0). Since we aim to determine the most accurate model between Model1 and Model2, we can choose to compare either B_r or B_θ at the centre of the system. The next subsections present these comparisons for B_r produced by radially and tangentially magnetized ASMs when their dimensions are changed. All these results obtained from the analytical models were programmed in Matlab.

A. Radially Magnetized Arc-shaped Permanent Magnet

We consider in Fig. 3 a radially magnetized ASM $A_1^{180^0}$ with magnetization grade $|\mathbf{M}|$ of 1.32 T (i.e., N45). We have taken the following dimensions in Fig. 3 (a): $\Delta r = r_2$-r_1 with r_1=30 mm and 30 mm<r_2<330 mm, Δz=30 mm with z_2=15 mm and z_1=-15 mm, $\theta_1=165^0$ and $\theta_2=195^0$. The dimensions used in Fig. 3 (b) are Δr =20 mm with r_1=30 mm and r_2=50 mm, z_2= $\Delta z/2$ mm and z_1= -$\Delta z/2$ mm with 0<Δz <300 mm, $\theta_1=165^0$ and $\theta_2=195^0$.

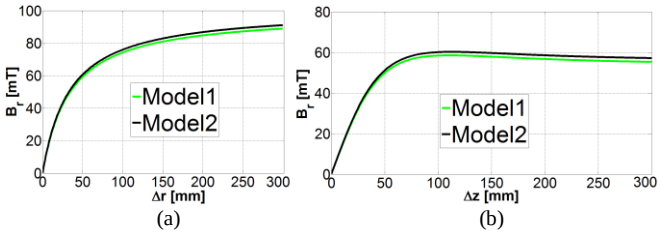

(a) (b)

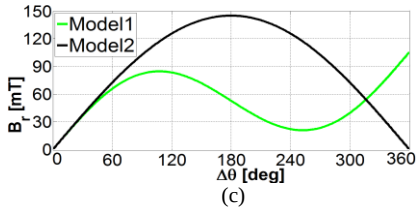

(c)

Fig. 3. Comparison of B_r at the centre of the system generated by an ASM $\mathbf{A_1^{180^0}}$ when (a) only $\Delta\mathbf{r}$ varies, (b) only $\Delta\mathbf{z}$ varies, (c) only $\Delta\boldsymbol{\theta}$ varies (B_{rmax}=145.12 [mT] and it occurs when $\Delta\boldsymbol{\theta}$=180^0 with Model2).

In Fig. 3 (c), we show the comparison of B_r when the angular width varies. We have taken the following dimensions: Δr=20 mm with r_1=30 mm and r_2=50 mm, Δz=30 mm with z_2=15 mm and z_1=-15 mm, $\theta_1=180^0-\Delta\theta/2$ and $\theta_2=\theta_1+\Delta\theta$ with $0^0<\Delta\theta<360^0$.

According to Fig. 3 (c), Model2 predicts higher values for B_r than the results from Model1 for $60^0<\Delta\theta<320^0$. For $\Delta\theta<60^0$, the results from both models are very similar. These analytical models also predict very similar results for B_r at the centre of the system when changes in Δr, and Δz, are made to $A_1^{180^0}$ whose angular width is 30^0, as shown in Figs. 3 (a) and (b). Since both models predict different results for $A_1^{180^0}$ when its angular width $\Delta\theta>60^0$, we want to compare B_r when changes in Δr, and Δz, are made to $A_1^{180^0}$ for an angular width of $\Delta\theta=90^0$ and for an angular width of $\Delta\theta=180^0$. These results are presented in Fig. 4, where we use r_1=30 mm.

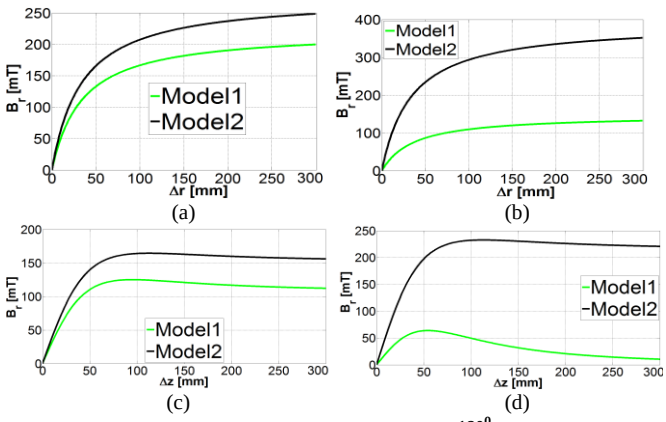

(a) (b) (c) (d)

Fig. 4. B_r at the centre of the system created by $\mathbf{A_1^{180^0}}$ when (a) only $\Delta\mathbf{r}$ varies ($\Delta\boldsymbol{\theta}$ =90^0, $\Delta\mathbf{z}=\mathbf{30\ mm}$), (b) only $\Delta\mathbf{r}$ varies ($\Delta\boldsymbol{\theta}$ =180^0, $\Delta\mathbf{z}=\mathbf{30\ mm}$), (c) only $\Delta\mathbf{z}$ varies ($\Delta\mathbf{r}=\mathbf{20\ mm}$, $\Delta\boldsymbol{\theta}$ =90^0), (d) only $\Delta\mathbf{z}$ varies ($\Delta\mathbf{r}=\mathbf{20\ mm}$, $\Delta\boldsymbol{\theta}$ =180^0).

We conclude that these models differ greatly when the angular width is increased. However, one of the advantages of Model1 is that it is a general model that can be used for arc-shaped magnets with any magnetization direction as long as the angular width is relatively small (approximately for $\Delta\theta<60^0$) as it is shown in Fig. 3. Furthermore, Figs. 3-4 suggest that by considering the results of Model2, B_r at the centre of the system is increased if the thickness, length and angular width are increased. However, an increment in such parameters will also increase the volume of the external magnetic system, which should be considered in a realistic application as this external magnetic system is to be moved by motors. Another interesting result from Fig. 3 (b) is that an optimal length of about 113 mm maximizes B_r at the centre of the system (B_{rmax}=60.3 mT with Model2). A longer length will not improve B_r.

B. Tangentially Magnetized Arc-shaped Permanent Magnet

We consider in Fig. 5 a tangentially magnetized ASM $A_3^{90^0}$ with magnetization grade $|\mathbf{M}|$ of 1.32 T (i.e., N45). We have taken the following dimensions in Fig. 5 (a): $\Delta r=r_2-r_1$ with r_1=30 mm and 30 mm<r_2<330 mm, Δz=30 mm with z_2=15 mm and z_1=-15 mm, $\theta_1=75^0$ and $\theta_2=105^0$. The dimensions used in Fig. 5 (b) are Δr=20 mm with r_1=30 mm and r_2=50 mm, $z_2=\Delta z/2$ mm and $z_1=-\Delta z/2$ mm with $0<\Delta z<300$ mm, $\theta_1=75^0$ and $\theta_2=105^0$.

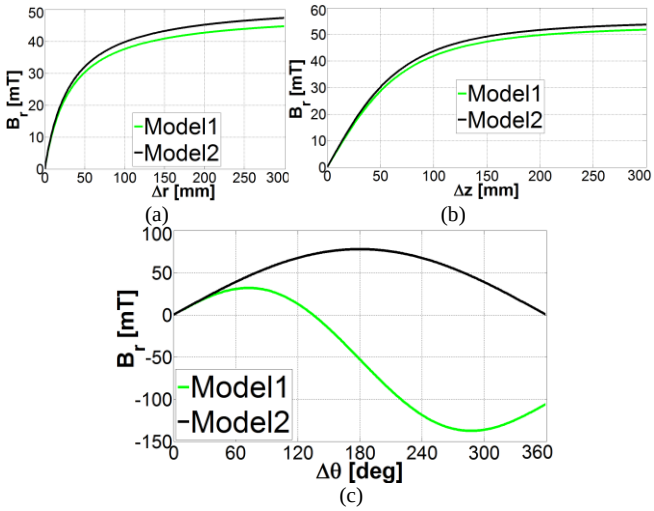

(a) (b) (c)

Fig. 5. Comparison of B_r at the centre of the system generated by an ASM $\mathbf{A_3^{90^0}}$ when (a) only $\Delta\mathbf{r}$ varies, (b) only $\Delta\mathbf{z}$ varies, (c) only $\Delta\boldsymbol{\theta}$ varies (B_{rmax}=78 [mT] and it occurs when $\Delta\boldsymbol{\theta}$=180^0 with Model2).

In Fig. 5 (c), we show the comparison of B_r when the angular width varies. We have taken the following dimensions: Δr=20 mm with r_1=30 mm and r_2=50 mm, Δz=30 mm with z_2=15 mm and z_1=-15 mm, $\theta_1=90^0-\Delta\theta/2$ and $\theta_2=\theta_1+\Delta\theta$ with $0^0<\Delta\theta<360^0$.

Figures 5 (a) and (b) show that both models predict similar results for B_r when changes in the thickness, Δr, and length, Δz, are made to $A_3^{90^0}$ whose angular width is 30^0. However, these models differ greatly when the angular width is increased beyond 60^0 as shown in Fig. 5 (c). The analytical results of Model2 also indicate that B_r is increased when the dimensions of the ASM are increased. Nevertheless, an angular width larger than 180^0 will not improve B_r. This optimal angular width is also obtained for a radially magnetized segment (see Fig. 3 (c)).

We also want to compare B_r when changes in Δr, and Δz, are made to $A_3^{90^0}$ for an angular width of $\Delta\theta=90^0$ and for an angular width of $\Delta\theta=180^0$. These results are presented in Fig. 6, where we use r_1=30 mm. Figure 6 shows that these analytical models differ when the angular width is larger than 60^0.

Since both analytical models differ greatly for radially and tangentially magnetized permanent magnets when their angular widths are larger than 60^0, we compare their theoretical results with experimental results to determine the

most accurate model that we can later use to conduct parametric studies and also find the optimal dimensions of the magnetic system that maximizes $|\mathbf{B}|$ at the centre of the system.

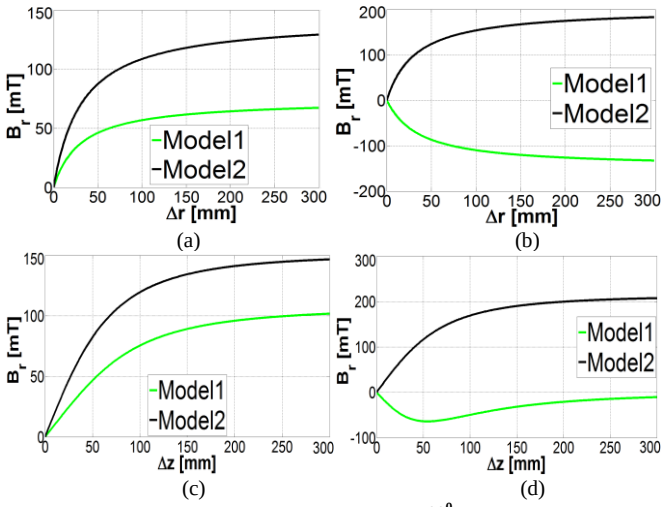

Fig. 6. B_r at the centre of the system created by $\mathbf{A_3^{90^0}}$ when (a) only $\Delta\mathbf{r}$ varies ($\Delta\boldsymbol{\theta}$ =90^0, $\Delta\mathbf{z} = \mathbf{30\ mm}$), (b) only $\Delta\mathbf{r}$ varies ($\Delta\boldsymbol{\theta}$ =180^0, $\Delta\mathbf{z} = \mathbf{30\ mm}$), (c) only $\Delta\mathbf{z}$ varies ($\Delta\mathbf{r} = \mathbf{20\ mm}, \Delta\boldsymbol{\theta}$ =90^0), (d) only $\Delta\mathbf{z}$ varies ($\Delta\mathbf{r} = \mathbf{20\ mm}, \Delta\boldsymbol{\theta}$ =180^0).

IV. OPTIMIZATION OF THE DRIVING MAGNETIC SYSTEM

A 3-channel Gauss meter (Lakeshore-Model 460) was used to measure the magnetic flux density generated by the arc-shaped magnets. The probe tip of the Gauss meter was mounted on plastic holders which were fabricated with a 3D printer. The probe tip of the Gauss meter can be moved along the X, Y and Z axes. These displacements are controlled by a micromanipulation system based on an X-Y-Z stage as shown in Fig. 7.

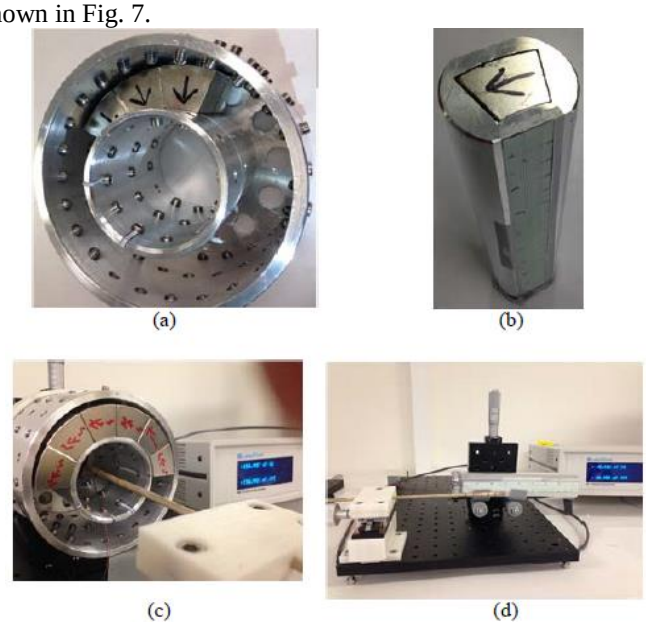

Fig. 7. Experimental setups with aluminum magnet cases to measure B_r when changes in $\Delta\theta$ and Δz are made, (a) Case1, (b) Case2, (c) Case1 mounted on the micromanipulation system, (d) Case2 mounted on the micromanipulation system.

A. *Accuracy of Analytical Models*

In our experiments with both ASMs $A_1^{180^0}$ and $A_3^{90^0}$, we used the following dimensions: Δr=20 mm with r_1=30 mm and r_2=50 mm, $\Delta\theta$=30^0, and Δz=30 mm with z_1=-15 mm and z_2=15 mm. The magnetization grade of each ASM $|\mathbf{M}|$ was 1.32 [T] (i.e., N45). Although any dimensions and magnetization grade can be chosen to verify the accuracy of the two analytical models, we decide to use these specific dimensions and magnetization grade because they are commercially available ASMs. With these dimensions, different arrays are possible by stacking up the segments along the z axis (i.e., increasing Δz), by placing them one next to the other and thus increasing $\Delta\theta$, or by a combination of increments in both dimensions. For instance, Fig. 8 shows the results for B_r generated by arrays of radially magnetized ASMs, while Fig. 9 shows the results for B_r created by arrays of tangentially magnetized ASMs.

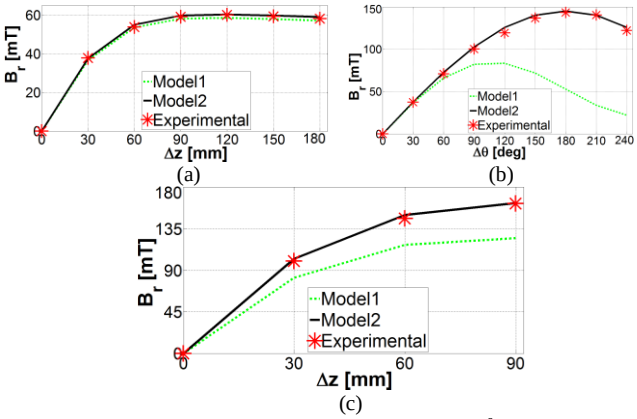

Fig. 8. B_r at the centre of the system created by $A_1^{180^0}$ when (a) only Δz varies ($\Delta\theta$ =30^0), (b) only $\Delta\theta$ varies (Δz=30 mm), (c) only Δz varies ($\Delta\theta$ =90^0).

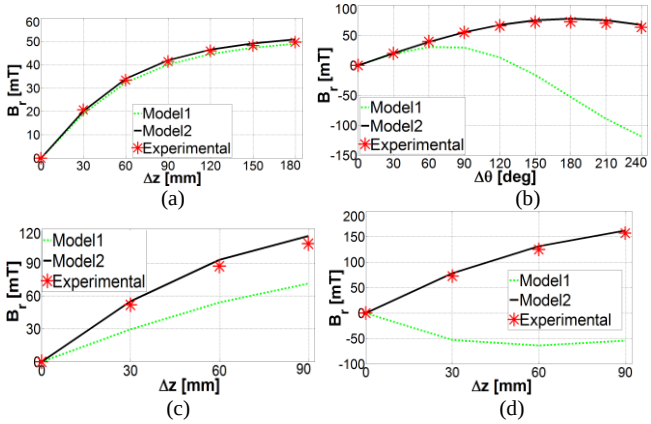

Fig. 9. B_r at the centre of the system created by $A_3^{90^0}$ when (a) only Δz varies ($\Delta\theta$ =30^0), (b) only $\Delta\theta$ varies (Δz=30 mm), (c) only Δz varies ($\Delta\theta$ =90^0), (d) only Δz varies ($\Delta\theta$ =180^0).

The results obtained in Figs. 8 and 9 indicate that Model2 is more accurate than Model1 in estimating B_r at the centre of the system, although when the angular width of the ASMs is 30^0, both models predict very similar results as shown in Fig. 8 (a) and Fig. 9 (a). Based on the accuracy of these analytical models, we use Model2 to conduct parametric

studies and the optimization of the driving magnetic system as it is presented in the next subsections.

B. Parametric Studies

We use Model2 to carry out parametric studies of ASMs radially and tangentially magnetized. The magnetization grade of each ASM $|\mathbf{M}|$ is 1.32 [T] and r_1=30 mm. Specifically, we are interested in determining the effects on B_r at the centre of the system due to changes in the three dimensions of the ASMs (i.e., Δr, $\Delta\theta$, and Δz**)**.

For an ASM $A_1^{180^0}$, we compute B_r at each point of the volumetric region defined by

$30\text{ mm} \leq r_2 \leq 200\text{ mm}$ (increments of 10 mm)
$10^0 \leq \Delta\theta \leq 360^0$ (increments of 10^0)
$20\text{ mm} \leq \Delta z \leq 400\text{ mm}$ (increments of 10 mm)

The results of B_r are shown in Fig. 10. It can be seen that B_r increases with increments of Δr and Δz. B_r also increases with increments of $\Delta\theta$ until $\Delta\theta$=180^0. For larger angular widths, B_r will decrease until it reaches zero [T].

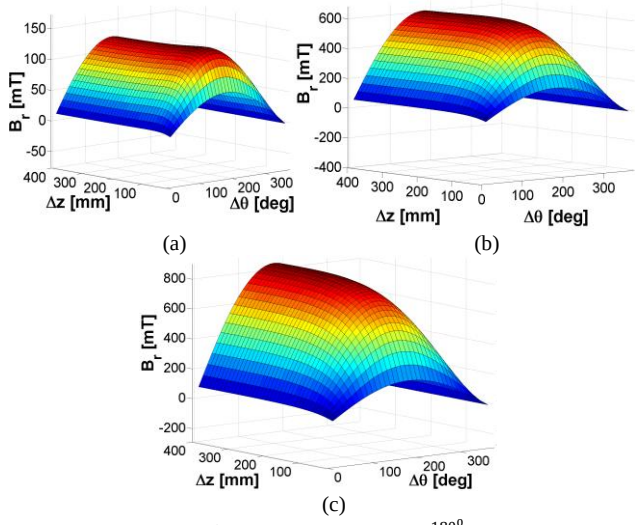

Fig. 10. B_r at the centre of the system created by $A_1^{180^0}$ when its dimensions are changed: (a) r_2=40 mm, (b) r_2=120 mm, c) r_2=200 mm.

Although, in general, B_r is improved as the dimensions of the ASM are increased (for $\Delta\theta < 180^0$), we want to determine the order of priority in which these dimensions should be increased to maximize B_r at the centre of the system. For this purpose, we use an Analysis of Variance (factorial ANOVA) to statistically determine the impact of each dimension on B_r [32]. The full ANOVA results are obtained with Minitab 17 in this study.

For the ANOVA of an ASM $A_1^{180^0}$, we use the following region of interest for its three dimensions:
$35\text{ mm} \leq r_2 \leq 135\text{ mm}$ (increments of 5 mm)
$9.549^0 \leq \Delta\theta \leq 180^0$ (increments of approx. 5^0)
$5\text{ mm} \leq \Delta z \leq 105\text{ mm}$ (increments of 5 mm)

The ANOVA results for these three parameters, which are presented under the column named "Source", are shown in Table 1, where the F value represents the mean square error to residual and is used to determine the significance of each parameter. The P value represents the significance level. Since the ANOVA study is conducted at 5% significance level, when the P value is less than 0.05, the effect of the respective parameter is significant to the response variable which in this case is B_r.

TABLE 1
THE ANOVA TABLE FOR B_r GENERATED BY $A_1^{180^0}$

Source	DF	Adj SS	Adj MS	F-Value	P-Value
Δr	20	38.39	1.91949	616.2	0.00
r_1*$\Delta\theta$	18	62.67	3.48193	1117.79	0.00
Δz	20	47.66	2.38316	765.05	0.00

As shown in Table 1, all parameters have the P-value of less than 0.05. Therefore, the three parameters significantly affect B_r at the 95% confidence interval. Furthermore, the highest F-value is on the angular width $\Delta\theta$, followed by the F-value on Δz, and lastly the F-value on Δr. These F values indicate that to increase B_r, it is more effective to firstly increase $\Delta\theta$, followed by increments in Δz and the last parameter to be increased is the thickness Δr of the ASM.

For an ASM $A_3^{90^0}$, we also compute B_r when the three dimensions are changed within the same volumetric region defined for the ASM $A_1^{180^0}$, and we also use r_1=30 mm. These results are shown in Fig. 11.

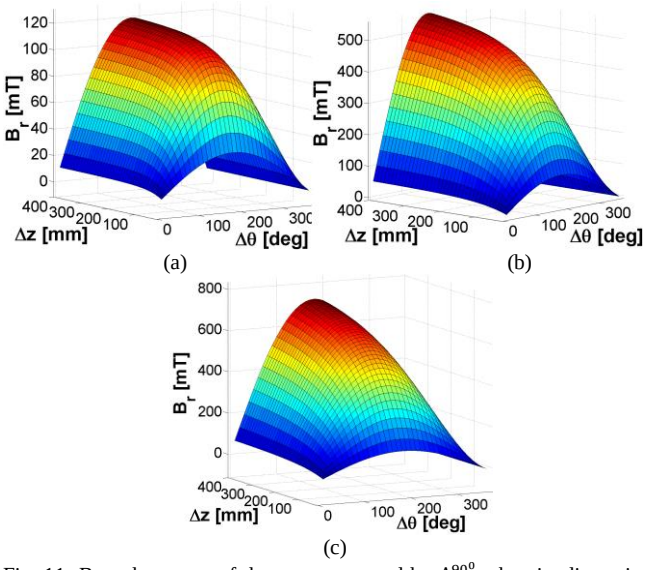

Fig. 11. B_r at the centre of the system created by $A_3^{90^0}$ when its dimensions are changed: (a) r_2=40 mm, (b) r_2=120 mm, (c) r_2=200 mm.

It can be seen from Fig. 11 that B_r increases with increments of Δr and Δz. B_r also increases with increments of $\Delta\theta$ until $\Delta\theta$=180^0. For larger angular widths, B_r will decrease until it reaches zero [T]. Furthermore, the order of priority in which these dimensions should be increased to maximize B_r at the centre of the system is obtained from the analysis of variance. For this analysis of variance, we also use the same region of interest defined for the ANOVA of an ASM $A_1^{180^0}$ and the results are presented in Table 2.

TABLE 2
THE ANOVA TABLE FOR B_r GENERATED BY $A_3^{90^0}$

Source	DF	Adj SS	Adj MS	F-Value	P-Value
Δr	20	12.42	0.62092	485.2	0.00
$r_2*\Delta\theta$	18	22.79	1.26588	989.17	0.00
Δz	20	23.56	1.17822	920.68	0.00

These F values reported in Table 2 indicate that to increase B_r, it is more effective to firstly increase $\Delta\theta$, followed by increments in Δz and the last parameter to be increased is the thickness Δr of the ASM.

With these parametric studies and ANOVA results carried out for ASMs $A_1^{180^0}$ and $A_3^{90^0}$, we determine the effects on B_r at the centre of the system due to changes in their three dimensions and also the order of priority in which they should vary. In the next subsection, we conduct optimization processes to find specific set of dimensions that maximize B_r.

C. Optimization of the Arc-Shaped Permanent Magnets

In this subsection, we present two optimization processes: the first one aims to maximize B_r for a given constant volume of the ASM (V_{asm}), while the second optimization process aims to minimize V_{asm} for a given constraint of desired B_r. Since Model2 represents an accurate analytical model that can be used for radially and tangentially magnetized ASMs with arbitrary dimensions and magnetization grade, we present the first optimization process considering the volume V_{asm} of $1.26\text{x}10^{-5}$ [m^3] as the given constraint. This is a typical volume of a commercial ASM $A_1^{180^0}$ (i.e., r_1=30 mm, r_2=50 mm, $\Delta\theta=30^0$ with $\theta_1=165^0$ and $\theta_2=195^0$, Δz=30 mm with z_1=-15 mm and z_2=15 mm, and $|\mathbf{M}|$= 1.32 [T]). Therefore, we aim to maximize B_r at the centre of the system created by $A_1^{180^0}$.

First optimization process:

Maximize $f(x)= B_r$
Subject to $h(x)= V_{asm} =1.26\text{x}10^{-5}$ [m^3]
Where

$f(x): \mathbb{R}^3 \rightarrow \mathbb{R}$

$x = [r_2, \Delta\theta, \Delta z]$

r_1 is fixed at 30 mm, but the other dimensions can take an arbitrary value. r_2 and Δz units are given in [mm] and the units for the angular width $\Delta\theta$ are given in degrees. We carry out the following step-by-step procedure:

1. Obtain the isosurface of a constant volume (Fig. 12 (a)).
2. Compute B_r at each point x (or vertex) that belongs to the isosurface (Fig. 12 (b)).
3. Calculate the maximum value of B_r (i.e., B_{rmax}) and find $x_{optimal}=[r_{2opt}, \Delta\theta_{opt}, \Delta z_{opt}]$ where the maximum occurs.

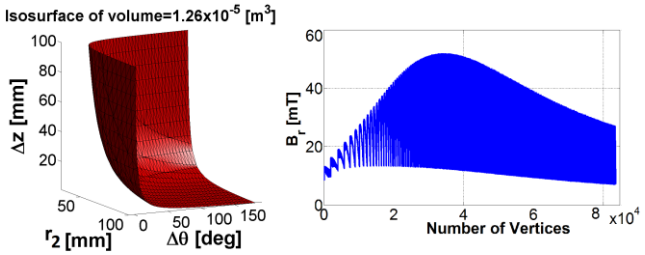

(a) (b)

Fig. 12. (a) Isosurface of constant volume, (b) B_r generated by each vertex that belongs to the isosurface.

By following the above procedure, we find: B_{rmax}=51.9 [mT], and $x_{optimal}$ =[37.9,100^0,27]. Therefore, r_{2opt}=37.9 mm, $\Delta\theta_{opt}=100^0$, $r_1 *\Delta\theta_{opt}$=52.4 mm, and Δz_{opt}=27 mm. These optimal dimensions for an ASM indicate that the volume of a single commercial ASM of volume $1.26\text{x}10^{-5}$ [m^3] is better distributed by allocating, firstly, more volume to the angular width dimension, followed by volume allocation to the ASM's length and finally to its thickness, because 52.4 mm>27 mm>7.9 mm. These results are in agreement with the ANOVA results in Table 1. Furthermore, a single commercial ASM $A_1^{180^0}$ generates only 37.5 [mT] at the centre of the system (see Fig. 8 (a)), but through this first optimization process we find that the same volume can be optimally distributed to generate a global optimal value of 51.9 [mT] (an improvement of about 38%). The inverse optimization process can be carried out to validate if B_{rmax} =51.9 [mT] is the global maximum.

Second optimization process:

Aiming to create B_r=51.9 [mT] with an ASM $A_1^{180^0}$, we attempt to find the minimum volume V_{min} (global minimum) required to generate such magnitude of flux density at the centre of the system. If V_{min} =$1.26\text{x}10^{-5}$ [m^3], then we are corroborating again that 51.9 mT is a global maximum (or global optimal).

Minimize $f(x)= V_{asm}$
Subject to $h(x)=B_r$=51.9 [mT]
Where

$f(x): \mathbb{R}^3 \rightarrow \mathbb{R}$

$x = [r_2, \Delta\theta, \Delta z]$

We carry out the following step-by-step procedure:
1. Obtain the isosurface of a constant magnetic flux density (Fig. 13 (a)).
2. Verify if each point x on the isosurface generates 51.9 mT at the centre of the system. To do this, we compute B_r at each vertex on the isosurface and obtain Fig. 13 (b).
3. Compute V_{asm} at each point x on the isosurface (see Fig. 13 (c)).
4. Calculate the minimum value of V_{asm} (i.e., V_{min}) and find $x_{optimal}=[r_{2opt}, \Delta\theta_{opt}, \Delta z_{opt}]$ where the minimum occurs.

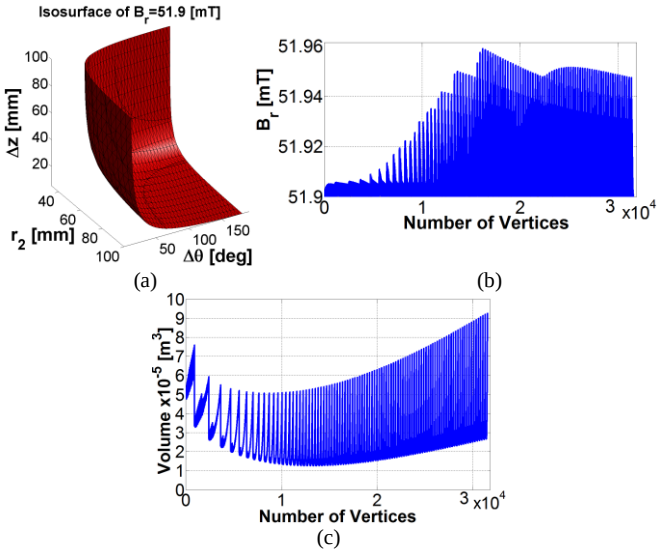

Fig. 13. (a) Isosurface of B_r=51.9 mT, (b) Br generated by each vertex, (c) volume of each vertex and the global minimum volume.

By following the above procedure, we find: V_{min} =1.255x10^{-5} [m^3], and $x_{optimal}$ =[38,99^0,27]. Therefore, r_{2opt}=38 mm, $\Delta\theta_{opt}$=99^0, and Δz_{opt}=27 mm. These results again confirm the optimal dimensions found from the first optimization process.

We also use the second optimization process to find the optimal dimensions and the minimum volume required to generate a flux density of 37.5 [mT] with an ASM $A_1^{180^0}$. We find that the minimum volume V_{min} of 8.1704x10^{-6} [m^3] can generate 37.5 [mT] at the centre of the system. This represents an improvement in the volume of the ASM of about 35%. This global minimum volume is reached for a unique set of dimensions: Δz=25 mm, Δθ=94^0, r_2=36 mm (and r_1 is fixed at 30 mm). By minimizing the volume, we will be able to more easily maneuver the external magnetic system while generating an adequate magnetic field to actuate the slider-crank mechanism embedded in the capsule robot. This is of particular interest when the dimensions of the driving magnetic system are scaled up to actuate the drug release module from an operating distance larger than r_1=30 mm which is the operating distance used in our prototype.

In the final parametric study, we progressively increase the volume of the ASM $A_1^{180^0}$ by multiplying the original volume of a single commercial ASM by a scaling factor. For each volume, we calculate B_{rmax} and $x_{optimal}$ by following the procedure explained for the first optimization process. Table 3 shows the results of a parametric study where the following increments are used: r_2: 0.5 mm, increments of Δθ: 1^0, and increments of Δz: 0.5 mm. By calculating $\Delta r_{opt} = r_{2opt} - r_1$ with r_1=30 mm, we obtain the results shown in Table 3.

From Table 3, we can see that the optimal distribution of the volume to generate a maximum B_r is obtained when the volume is allocated firstly along the angular width, secondly along the length and thirdly along the thickness. These results for optimal volume allocation are consistent with the ANOVA results in Table 1.

TABLE 3
VARIATION OF B_{rmax} DUE TO CHANGES IN THE VOLUME OF THE ASM $A_1^{180^0}$. |**M**|= 1.32 [T]

Scaling Factor	Δr_{opt} [mm]	$\Delta\theta_{opt}$ [deg]	$r_1 * \Delta\theta_{opt}$ [mm]	Δz_{opt} [mm]	B_{rmax} [mT]
1	7.9	100.0	52.4	27.0	51.9
2	11.1	112.0	58.6	32.5	84.1
3	13.8	118.0	61.8	36.0	109.0
4	16.0	122.0	63.9	38.8	129.7
5	17.9	126.0	66.0	41.0	147.4
6	19.5	128.1	67.1	43.5	163.0
7	21.0	131.0	68.6	45.2	176.9
8	22.5	133.0	69.6	46.7	189.6

We also use the first optimization process for an ASM $A_3^{90^0}$ with a commercial volume V_{asm} of 1.26x10^{-5} [m^3] and r_1=30 mm. We find: B_{rmax}=28.5 [mT], and $x_{optimal}$ =[36.47,93^0,36]. Therefore, r_{2opt}=36.47 mm, $\Delta\theta_{opt}$=93^0, and Δz_{opt}=36 mm. This B_{rmax} is a global maximum. A single commercial ASM $A_3^{90^0}$ generates only 20 [mT] at the centre of the system (see Fig. 9 (a)), but we find that the same volume can be optimally distributed to generate a global optimal value of 28.5 [mT] (an improvement of about 42.5%).

We also progressively increase the volume of the ASM $A_3^{90^0}$ by multiplying the original volume of a single commercial ASM by a scaling factor. For each volume, we calculate B_{rmax} and $x_{optimal}$ by following the procedure explained for the first optimization process. Table 4 shows the results of a parametric study where the following increments are used: r_2: 0.5 mm, increments of Δθ: 1^0, and increments of Δz: 0.5 mm. By calculating $\Delta r_{opt} = r_{2opt} - r_1$ with r_1=30 mm, we obtain the results shown in Table 4.

TABLE 4
VARIATION OF B_{rmax} DUE TO CHANGES IN THE VOLUME OF THE ASM $A_3^{90^0}$. |**M**|= 1.32 [T]

Scaling Factor	Δr_{opt} [mm]	$\Delta\theta_{opt}$ [deg]	$r_1 * \Delta\theta_{opt}$ [mm]	Δz_{opt} [mm]	B_{rmax} [mT]
1	6.5	93.0	48.7	36.0	28.5
2	9.0	105.0	55.0	44.2	47.4
3	11.0	111.7	58.5	49.5	62.6
4	12.8	115.9	60.7	53.5	75.5
5	14.2	119.0	62.3	57.5	86.8
6	15.5	122.0	63.9	60.5	96.9
7	16.7	123.9	64.9	63.5	106.0
8	17.8	126.1	66.0	66.0	114.4

From Table 4, we can see that the optimal distribution of the volume to generate a maximum B_r is obtained when the volume is allocated firstly along the angular width, secondly along the length and thirdly along the thickness. These are the same results obtained from the analysis of variance in Table 2.

The results reported in Tables 3 and 4 show that for the same volume, radially magnetized segments always produce higher magnetic flux densities at the centre of the system than the flux densities produced by tangentially magnetized

segments. However, in our next section, we work with the worst scenario, and therefore we only use tangentially magnetized ASMs to experimentally verify the efficacy of the proposed optimization method.

V. EXPERIMENTAL METHODS

A. Magnetic Flux Density

We can use the results reported in Tables 3 and 4 to fabricate magnetic systems with optimal dimensions that can maximize B_r at the centre of the system. For instance, different arrays can be obtained with five commercial ASMs tangentially magnetized. We present two possible configurations in Figs. 14 (a) and (b), which generate the theoretical values of 49.2 [mT] and 75.3 [mT] at the centre of the system, respectively. However, for the same volume, we obtain from Table 4 the optimal dimensions (shown in Fig. 14 (c)) of a single ASM that can generate a theoretical flux density of 86.8 [mT]. The magnetic structure shown in Fig. 14 (a) has a poor distribution of its volume along its three dimensions, and that is the reason why it only generates 49.2 [mT]. On the other hand, the magnetic structure shown in Fig. 14 (b) has a better distribution of its volume along its three dimensions by allocating most of the volume to its angular width, followed by volume allocation along the length and the smallest dimension given to its thickness. For this reason, this magnetic structure produces a higher flux density of 75.3 [mT].

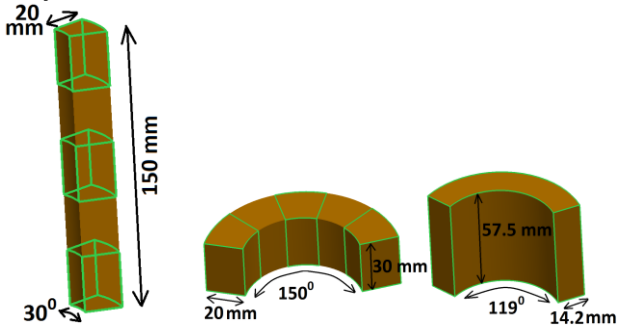

Fig. 14. Magnetic structures with the same volume of $5*V_{asm}$. (a) array of 5 commercial segments placed one on top of the other, (b) 5 segments are arranged one next to the other, (c) optimal dimensions of a single ASM $A_3^{90^0}$.

The closer is the dimensions of the magnetic structure to the optimal dimensions, the higher will be the magnetic flux density. The specific optimal dimensions shown in Fig. 14 (c) could be customized by a manufacturer. However, we have decided to implement the magnetic structure shown in Fig. 14 (b) to reduce costs and used the symmetry of the system to double the magnitude of the flux density at the centre of the system. This implementation is shown in Fig. 15 (a).

If we customized the magnetic structure with two tangentially magnetized segments $A_3^{90^0}$ and $A_4^{270^0}$, each segment with the optimal dimensions presented in Table 4 (using the scaling factor 5) and also depicted in Fig. 14 (c), we would obtain the flux density B_x along the x axis as shown in Fig. 15 (b) (the black line), where B_x=86.8*2=173.6 [mT] at the centre of the system (note that B_x=B_r along the x axis).

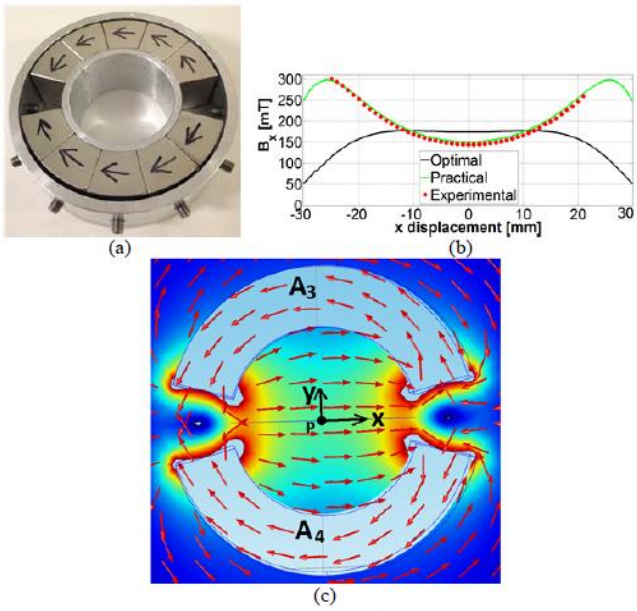

Fig. 15. (a) Magnetic structure made of only tangentially magnetized segments of the types A_3 and A_4, (b) B_x along the x axis created by: an optimal magnetic system (black line) and the practical magnetic system shown in Fig. 15 (a) (theoretical results using Model2: green line, and experimental results: the dotted red line), (c) Vector field of the magnetic flux density norm on the plane z=0 generated by the structure shown in Fig. 15 (a).

However, for practical reasons we assembled the magnetic structure shown in Fig. 15 (a) and we measured B_x along the x axis as shown in Fig. 15 (b) (the dotted red line), where B_x=144.2 [mT] at the centre of the system. The optimal dimensions of the magnetic system would generate an approximately constant B_x in the range -17 mm<x<17 mm which is advantageous to guarantee a stable transmitted peak torque on the IPM regardless of its position within that range of operation. On the other hand, the practical assembly of the magnetic system generates a U-shape B_x curve with a minimum experimental value of 144.2 [mT] at x=0. This result from the practical assembly indicates that the IPM will experience a minimum peak torque if it is located at the centre of the system, but if it's moved from the centre, the transmitted peak torque will increase proportionally.

The analytical results show that B_y is 0 [mT] along the x axis for the magnetic structure shown in Fig. 15 (a). For this reason, we do not show B_y in any results. However, we present in Fig. 15 (c) a 2D vector field representation of $|\mathbf{B}|$ created by such a magnetic structure in plane z=0 (using Comsol). The magnitude of this vector representation was normalized just to show the direction of **B** around the point P. Fig. 15 (c) shows that $|\mathbf{B}|$ approximates B_x over a relatively large region around point P (i.e., the centre of the system). Therefore, the B_x component is mainly responsible for the transmitted torque on the IPM in (1). We present in the next section, the experimental results for the transmitted torque on the IPM with the practical assembly shown in Fig. 15 (a).

B. Magnetic Torque

A torque gauge (HTG2-40 supplied by IMADA) with its respective torque sensor held in place a 3.1 mm cubic IPM

with magnetization grade N50 (i.e,$|\mathbf{m}|$=1.4 [T]). The IPM was connected to the torque sensor via a plastic connector that was manufactured using a 3D printer. The torque sensor was mounted on plastic holders which were also fabricated using a 3D printer and could be moved along the X axis. The driving magnetic system was mounted on a plastic holder that possesses 30^0 angle indicators and allows its manual rotation about the Z axis. This driving magnetic system, once mounted on the plastic holder, could be moved along the Y and Z axes. These displacements were controlled by a micromanipulation system based on an X-Y-Z stage as shown in Fig. 16 (a).

In the first experiment, we positioned the IPM'centre at the centre of the system with its magnetization vector **m** aligned with the X axis (see Fig. 16 (a)), and we manually rotated the driving magnetic system about the Z axis every 30^0 until a full cycle was completed. The theoretical and experimental results of the transmitted torque on the IPM τ_z are shown in Fig. 16 (b). It can be seen that the peak torque is transmitted to the IPM when the misalignment angle $\emptyset_m$ between **m** and **B** reaches 90^0. The theoretical results were estimated with (1) where **B** is calculated using Model2. In the second experiment, the IPM's centre was moved along the X axis with increments of 3 mm and its magnetization vector **m** was aligned with the Y axis along the entire trajectory. In this second experiment, the driving magnetic system was never rotated to guarantee that $\emptyset_m=90^0$ and a peak torque were transmitted at all times. The results from the second experiment are shown in Fig. 16 (c).

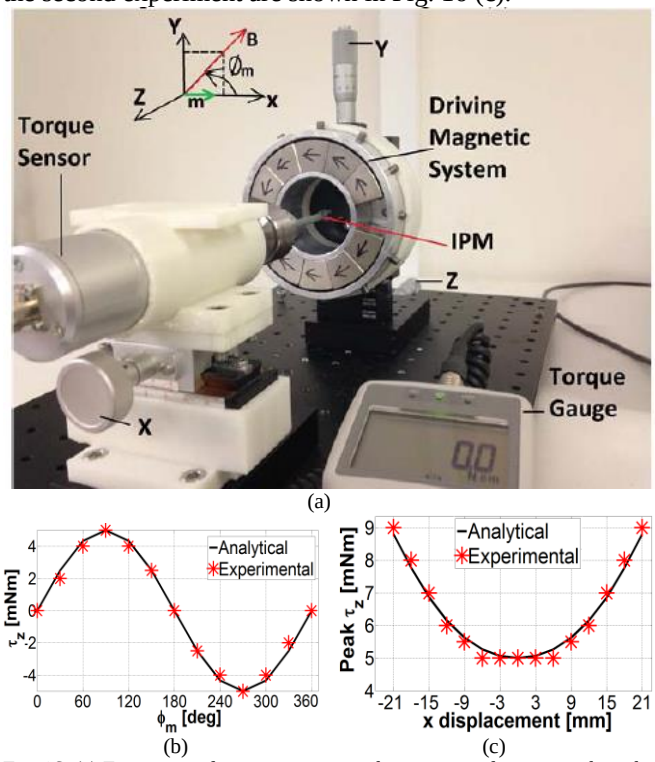

Fig. 16. (a) Experimental setup to measure the transmitted torque to the cubic IPM by the driving magnetic system made of 5 ASMs A_3 and 5 ASMs A_4, (b) τ_z imparted to the IPM (an experimental peak torque of 5 [mNm] is reached at $\emptyset_{\mathbf{m}} = 90^0$), (c) Peak torque transmitted to the IPM as its centre is moved along the x axis.

These experimental results for the transmitted torque on the IPM show that the minimum peak torque of 5 [mNm] is obtained when the IPM's centre coincides with the centre of the system, and the peak torque is further improved if the IPM's centre is located at any other position in the X axis. If the driving magnetic system were customized with two tangentially magnetized ASMs, each with the optimal dimensions shown in Fig. 14 (c), we would obtain an approximately constant theoretical peak torque of 6 [mNm] in the range -17 mm<x<17 mm because the IPM would be under an approximately uniform B_x of 173.6 [mT] in the same range. If the IPM's centre was located outside that range of operation (i.e., x<-17 mm or x>17 mm), the peak torque would decrease and the driving magnetic system may need to be repositioned so that the IPM's centre can fall again within the adequate region of operation.

Although these driving magnetic systems made of only tangentially magnetized segments can be fabricated by assembling commercially available ASMs or by customizing the ASMs with optimal dimensions, in either case, the imparted peak torque to the IPM is at least 5 [mNm] within the region of operation. However, two additional facts should be considered when this magnetic system is scaled up [16]: 1) 5 [mNm] is more than enough peak torque to actuate the piston of the drug release module, knowing that 3.5 [mNm] is sufficient for the release, 2) a peak torque is not always required to actuate the piston. For instance, magnetic torques of 2 and 4 [mNm], which can be obtained when $\emptyset_{\mathbf{m}}=30^0$ and $\emptyset_{\mathbf{m}}=60^0$, respectively, are also adequate to release a variety of drug compounds. Furthermore, if the driving magnetic system was fabricated by only assembling radially magnetized ASMs, the peak torque on the IPM at the centre of the system will be higher than the peak torque generated with the driving magnetic system made of only tangentially magnetized ASMs because radially magnetized ASMs can produce higher flux densities as suggested by the results depicted in Tables 3 and 4.

We estimate, for example, that with the same volume of 5 commercial segments of the type A_1 and 5 the type A_2, it is possible to generate B_x=294.8 [mT] at the centre of the system (see Table 3 with scaling factor of 5: B_{rmax}=147.4 [mT], and therefore B_x=2* B_{rmax}). This higher flux density would allow an increase in the operating distance. In addition, this optimal magnetic structure made of only radially magnetized ASMs would impart a peak torque of approximately 10 [mNm] to the IPM. This higher peak torque would allow a further miniaturization of the IPM. However, if we wanted to impart a peak torque between 5 to 6 [mNm] with an optimal driving system made of only radially magnetized ASMs, we would select only two segments (A_1 and A_2), each with the optimal dimensions presented in Table 3 (using the scaling factor 2: B_{rmax}=84.1 [mT], and therefore B_x=168.2 [mT]=2* B_{rmax}). This selection implies a reduction of 60% ($\frac{5-2}{5}$*100%) in the volume if compared with the optimal dimensions of 2 tangentially magnetized ASMs, each with the dimensions shown in Fig. 14 (c). These results clearly indicate that the driving magnetic system can be scaled up with optimal dimensions

to minimize its total volume while generating adequate flux densities and magnetic torques to actuate the drug release module embedded in the capsule robot. Consequently, a minimum volume of the driving magnetic system will improve its maneuverability and reduce fabrication costs.

VI. Conclusion and Future Work

The optimization of both the IPM and the driving magnetic system is important to obtain an efficient magnetic linkage (i.e., an optimized magnetic field and torque imparted to the IPM) while minimizing the dimensions of the IPM to be embedded in the capsule robot and at the same time minimizing the volume of the driving magnetic system to improve its maneuverability and reduce its fabrication cost. Furthermore, the size optimization of the driving magnetic system not only helps to minimize its volume but also allows larger operating distances to actuate the IPM and enables further miniaturization of the IPM.

In this paper, we focus on the optimization of the driving magnetic system which consists of an array of arc-shaped permanent magnets. Specifically, we found optimal dimensions for the driving magnetic system (i.e., thickness, angular width and length) and obtained an optimized magnetic field and subsequently a magnetic torque. This was carried out by using a very accurate analytical model, called Model2, which allows a fast global optimization and is useful for any arbitrary dimension of the ASM. Due to its high accuracy, Model2 can be used to scale up the driving magnetic system which is necessary for the final application where larger operating distances are needed. We found that Model1 was not accurate in predicting the flux density if the angular width of the ASM was larger than 60^0.

We have also found, through parametric studies and a statistical analysis (ANOVA), efficient ways to distribute the volume of the ASMs. Specifically, we have found that for both radially and tangentially ASMs, it is always more efficient to firstly increase $\Delta\theta$, followed by increments in Δz and the last parameter to be increased is the thickness Δr. In this order of priority, the volume can be minimized while obtaining higher flux densities and magnetic torques in the centre of the system where the IPM is located. Our results also indicate that optimal radially magnetized ASMs always generate higher flux densities than what can be generated with optimal tangentially magnetized ASMs. Although in this work we have presented driving magnetic systems made of segments with only one type of magnetization direction (either radially or tangentially magnetized ASMs), it is also possible to fabricate driving magnetic systems with a combination of both types of ASMs. However, the optimization of such a magnetic structure is part of our future work.

ACKNOWLEDGMENTS

This work was supported in part by the Intelligent Nano-Tera Research Systems Laboratory. The work of F. Munoz was supported by a Ph.D. scholarship from the University of Wollongong Research Council.

References

[1] R. G. Montague, C. Bingham, and K. Atallah, "Magnetic Gear Pole-Slip Prevention Using Explicit Model Predictive Control," *IEEE/ASME Transactions on Mechatronics*, vol. 18, pp. 1535-1543, Oct. 2013.

[2] M. Simi, G. Gerboni, A. Menciassi, and P. Valdastri, "Magnetic torsion spring mechanism for a wireless biopsy capsule," *ASME J. Med. Devices*, vol. 7, Dec. 2013.

[3] C. D. Natali, J. Buzzi, N. Garbin, M. Beccani, and P. Valdastri, "Closed-Loop Control of Local Magnetic Actuation for Robotic Surgical Instruments," *IEEE Transactions on Robotics*, vol. 31, pp. 143-156, Feb. 2015.

[4] P. Vartholomeos, C. Bergeles, L. Qin, and P. E. Dupont, "An MRI-powered and controlled actuator technology for tetherless robotic interventions " *International Journal of Robotics Research* vol. 32, pp. 1536-1552, Nov. 2013.

[5] M. Naganuma, N. Hosoe, and H. Ogata, "Inflammatory bowel disease and novel endoscopic technologies," *Digestive Endoscopy*, vol. 26, pp. 20-28, 2014.

[6] S. Yim, E. Gultepe, D. Gracias, and M. Sitti, "Biopsy using a Magnetic Capsule Endoscope Carrying, Releasing and Retrieving Untethered Micro-grippers," *IEEE Trans. on Biomedical Engineering*, Sep. 2013.

[7] J. L. Gorlewicz, S. Battaglia, B. F. Smith, G. Ciuti, J. Gerding, A. Menciassi, K. L. Obstein, P. Valdastri, and R. J. Webster, "Wireless Insufflation of the Gastrointestinal Tract," *IEEE Trans. Biomedical Engineering*, vol. 60, May. 2013.

[8] G. S. Lien, C. W. Liu, J. A. Jiang, C. L. Chuang, and M. T. Teng, "Magnetic Control System Targeted for Capsule Endoscopic Operations in the Stomach—Design, Fabrication, and in vitro and ex vivo Evaluations," *IEEE Transactions on Biomedical Engineering*, vol. 59, pp. 2068-2079, Jul. 2012.

[9] A. W. Mahoney and J. J. Abbott, "Five-degree-of-freedom manipulation of an untethered magnetic device in fluid using a single permanent magnet with application in stomach capsule endoscopy," *The International Journal of Robotics Research*, pp. 1-19, 2015.

[10] Z.-J. Sun, X.-G. Cheng, S. Cao, B. Ye, H.-H. Zhang, and S. Liu, "Multi-applications of a Magnet Configuration in Actuating Capsule Endoscope," *IEEE/ASME International Conference on Advanced Intelligent Mechatronics (AIM)*, pp. 106-111, July 8-11 2014.

[11] Z.-J. Sun, B. Ye, Y. Qiu, X.-G. Cheng, H.-H. Zhang, and S. Liu, "Preliminary Study of a Legged Capsule Robot Actuated Wirelessly by Magnetic Torque," *IEEE Transactions on Magnetics*, vol. 50, August 2014.

[12] S. Yim and M. Sitti, "Design and Rolling Locomotion of a Magnetically Actuated Soft Capsule Endoscope," *IEEE Transactions on Robotics*, vol. 28, pp. 183-194, Feb. 2012.

[13] S. Yim and M. Sitti, "Shape-programmable soft capsule robots for semi-implantable drug delivery," *IEEE Trans. Robot*, vol. 28, pp. 1198-1202, Oct. 2012.

[14] F. Munoz, G. Alici, and W. Li, "A review of drug delivery systems for capsule endoscopy " *Advanced Drug Delivery Reviews*, vol. 71, pp. 77-85, May 2014.

[15] F. Munoz, G. Alici, and W. Li, "Design Optimization of a Magnetomechanical System for Drug Delivery in Wireless Capsule Endoscopy," *IEEE/ASME International Conference on Advanced Intelligent Mechatronics*, pp. 1097-1102, July 08 2014.

[16] F. Munoz, G. Alici, and W. Li, "A Magnetically Actuated Drug Delivery System for Robotic Endoscopic Capsules," *ASME Journal of Medical Devices*, Vol.10, pp. 011004-1-11, March 2016.

[17] F. Munoz, G. Alici, and W. Li, "Optimization of Multiple Arc-shaped Magnets for Drug Delivery in a Capsule Robot," *IEEE/ASME International Conference on Advanced Intelligent Mechatronics*, pp. 189-195, Busan, Korea, July 2015.

[18] J. S. Agashe and D. P. Arnold, "A study of scaling and geometry effects on the forces between cuboidal and cylindrical magnets using analytical force solutions " *Journal of Physics D: Applied Physics*, vol. 41, pp. 1-9, May 2008.

[19] Y. Shen, "Novel Permanent Magnet Brushless Machines Having Segmented Halbach Array," Doctor of Philosophy, Department of Electronic and Electrical Engineering, The University of Sheffield, Sheffield, UK, 2012.

[20] M. Simi, M. Silvestri, C. Cavallotti, M. Vatteroni, P. Valdastri, A. Menciassi, and P. Dario, "Magnetically Activated Stereoscopic Vision System for Laparoendoscopic Single-Site Surgery," *IEEE/ASME Transactions on Mechatronics*, vol. 18, pp. 1140-1151, Jun. 2013.

[21] H. Zhou, G. Alici, T. Than, and W. Li, "Modeling and experimental investigation of rotational resistance of a spiral-type robotic capsule inside a real intestine," *IEEE/ASME Transactions on Mechatronics,* vol. 18, pp. 1555 – 1562, October 2013.
[22] H. Zhou, G. Alici, T. Than, and W. Li, "Modeling and experimental characterization of propulsion of a spiral-type microrobot for medical use in gastrointestinal tract," *IEEE Transactions on Biomedical Engineering,* vol. 60, pp. 1751 – 1759, June 2013.
[23] T. D. Than, G. Alici, H. Zhou, and W. Li, "A review of localization systems for robotic endoscopic capsules," *IEEE Transactions on Biomedical Engineering,* vol. 59, pp. 2387-2399, Sep. 2012.
[24] T. D. Than, G. Alici, S. Harvey, H. Zhou, and W. Li, "Concept and simulation study of a novel localization method for robotic endoscopic capsules using multiple positron emission markers," *Medical Physics,* vol. 41, July 2014.
[25] T. D. Than, G. Alici, S. Harvey, G. O'Keefe, H. Zhou, W. Li, T. Cook, and S. Alam-Fotias, "An effective localization method for robotic endoscopic capsules using multiple positron emission markers " *IEEE Transactions on Robotics* vol. 30, pp. 1174-1186, 1 October 2014.
[26] D. C. Jiles, "Introduction to magnetism and magnetic materials," *Second Edition,* Jun. 1998.
[27] F. Carpi and H. Shaheed, "Gran challenges in magnetic capsule endoscopy," *Expert Rev. Med. Devices,* vol. 10, pp. 433-436, Jul. 2013.
[28] R. Ravaud and G. Lemarquand, "Magnetic field created by uniformly magnetized tile permanent magnet," *Progress in Electromagnetics Research B,* vol. 24, pp. 17-32, 2010.
[29] E. P. Furlani, S. Reznik, and A. Kroll, "A Three-Dimensional Field Solution for Radially Polarized Cylinders," *IEEE Transactions on Magnetics,* vol. 31, pp. 844-851, Jan. 1995.
[30] R. Ravaud and G. Lemarquand, "Comparison of the coulombian and amperian current models for calculating the magnetic field produced by radially magnetized arc-shaped permanent magnets," *Progress in Electromagnetics Research,* vol. 95, pp. 309-327, 2009.
[31] R. Ravaud and G. Lemarquand, "Analytical Expression of the Magnetic Field Created by Tile Permanent Magnets Tangentially Magnetized and Radial Currents in Massive Disks," *Progress In Electromagnetics Research B,* vol. 13, pp. 309-328, 2009.
[32] Q. WU, "A Study of the Laser Milling Process for Polycrystalline Diamonds," *Ph.D. Thesis,School of Mechanical and Manufacturing Engineering, The University of New South Wales, NSW, Australia,* Aug 2013.